IEEE Access
Multidisciplinary ⋮ Rapid Review ⋮ Open Access Journal

Received 8 February 2023, accepted 23 February 2023, date of publication 31 March 2023, date of current version 13 April 2023.

Digital Object Identifier 10.1109/ACCESS.2023.3263794

APPLIED RESEARCH

Low Complexity Compact Lowpass Filter Using T-Shaped Resonator Loaded With a Stub

MOHSEN HAYATI[1], REZVAN SALAHI[2], MARYAM AKBARI[3], SIAMAK ZARGARI[2], AND DEREK ABBOTT[4], (Fellow, IEEE)

[1]Department of Electrical Engineering, Faculty of Engineering, Razi University, Kermanshah 67144-14971, Iran
[2]Department of Electrical Engineering, Amirkabir University of Technology (Tehran Polytechnic), Tehran 15875-4413, Iran
[3]Department of Electrical Engineering, Iran University of Science and Technology, Tehran 16846-13114, Iran
[4]School of Electrical and Electronic Engineering, The University of Adelaide, Adelaide, SA 5005, Australia

Corresponding author: Mohsen Hayati (mohsen_hayati@yahoo.com)

ABSTRACT A novel miniaturized microstrip low pass filter (LPF) with a wide stopband and sharp roll-off is presented. The designed filter is developed by realizing a T-shaped structure loaded with a stub as a resonator and open-stubs as suppressor cells to achieve a simple structure for ease of fabrication process. The new filter with a symmetrical structure has a 3 dB cut-off frequency of 2.15 GHz, the transition band is 123 dB/GHz from −3 dB to −40 dB, a stopband with an attenuation level better than −20 dB from 2.4 up to 22.1 GHz with a compact size of $0.0132\lambda_g{}^2$. The insertion loss in the passband is less than 0.3 dB and return loss is lower than −20 dB. The filter is fabricated, and the results show agreement between the simulation and measurement.

INDEX TERMS Microstrip lowpass filter (LPF), resonators, stubs, suppressor cells.

I. INTRODUCTION

With the rapid development of microwave systems, in recent years, the demand for microstrip filters with improved specifications has increased. Most of the published low pass filters (LPFs) have attempted to focus on either improving parameters such as sharpness by designing a new resonator or eliminating further harmonics and broadening bandwidth by designing suppressor cells. However, improving each parameter usually affects the other parameters, and it is challenging to achieve a filter with desirable characteristics such as sharp roll-off, wide bandwidth, small size, etc. all at the same time.

In [1], an ultra-wide stopband LPF using a T-shaped resonator and folded structure is presented. Although this LPF uses a folded structure to achieve a compact size, the filter size is still large. Also, the use of multiple resonators to achieve an ultra-wide stopband has led to the complexity in the design. Moreover, the return loss and the roll-off rate are not appropriate for this LPF. A defected ground structure (DGS) has been used in [2] to extend the stop bandwidth, but the use of this method increases complexity. In addition, other LPF features, such as roll-off, suppression factor, and return loss, have room for improvement. High suppression level in the stopband by utilizing Chebyshev structures is presented in [3], [4], [5], and [6]. However, all of them suffer from low return loss and lack of sharpness in the transition band. A modified rectangular-shaped LPF is presented in [7]. Though the group delay is desirable in this LPF, some parameters such as return loss and roll-off require improvement. A microstrip filter with very sharp roll-off, wide stopband, and required selectivity using a split-ring resonator loaded by folded patches is reported in [8]. However, the relatively large size is the drawback of this filter.

Ultra-sharp roll-off rate LPFs are reported in [9] and [10], but the stopband is narrow. Desirable filter specifications such as sharp transition band, high suppressor level, and wide stopband are reported in [11] and [12], but this is at the expense of a significant increase in filter size. A compact microstrip LPF with a very flat group delay in the passband is designed and fabricated in [13]. The gradual roll-off is the most critical drawback of this filter. A harmonic suppressor cell with miniaturized size, flat group delay, but with gradual roll-off is presented in [14]. In [15], an LPF with wide stopband, small footprint and low insertion loss using a stepped

The associate editor coordinating the review of this manuscript and approving it for publication was Li Yang.

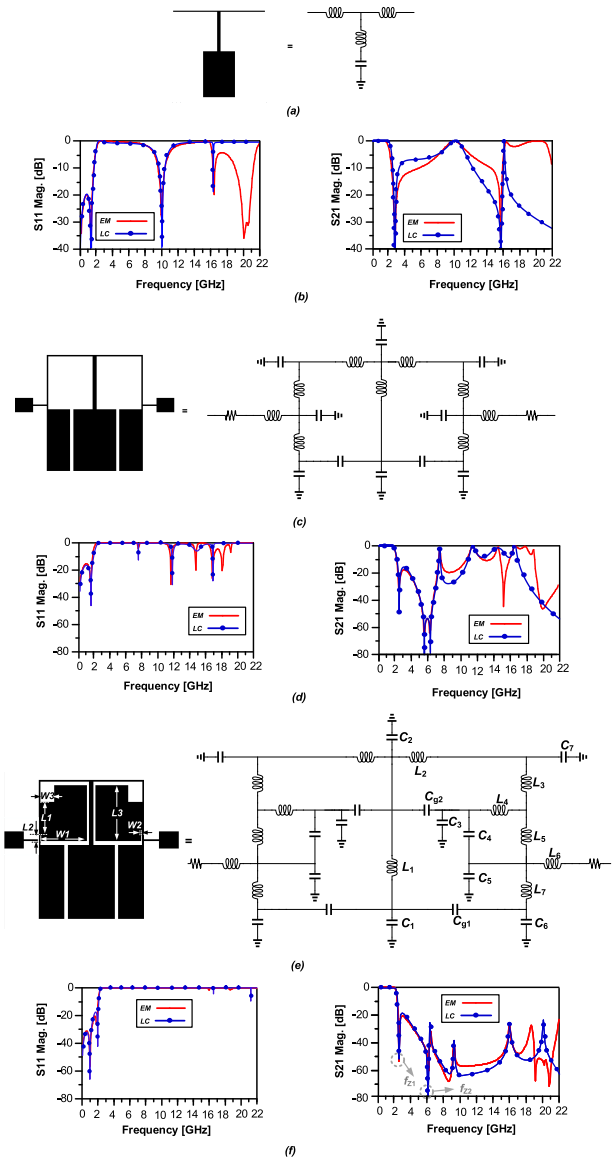

FIGURE 1. Layout and simulated S-parameters (a,b) proposed T shaped resonator loaded with stub. (c,d) Resonator with suppressor cell-1. (e,f) Resonator with suppressor cell-1. (LC values for resonator in Fig. 1(e): $L_1 = 2.43$, $L_2 = 2.02$, $L_3 = 1.05$, $L_4 = 1.04$, $L_5 = 1.38$, $L_6 = 1.147$, $L_7 = 0.1797$, $C_1 = 1245$, $C_{g1} = 99.35$, $C_2 = 12.16$, $C_{g2} = 125.95$, $C_3 = 181$, $C_4 = 25.61$, $C_5 = 15$, $C_6 = 1503$, $C_7 = 50.73$). Units: L, nH; C, fF.

impedance hairpin resonator is presented, with gradual roll-off. An LPF composed of symmetrically loaded resonant patches is presented in [16] for obtaining an extended stop-band and narrow bandpass, but has a complex structure and slow transition band. A five order Chebyshev LPF presented in [17] has a sharp roll-off and narrow passband, whereby cascading the LPF with three asymmetric units, the suppression level and stopband are improved, but the filter has a large size. In [18], an LPF using an embedded band-stop structure to obtain a wide stopband is presented, but suffers from the large size, and a narrow stopband. Modified ring resonators have been used in [19] to improve the transition band. Moreover, to attain an ultra-wide stopband,

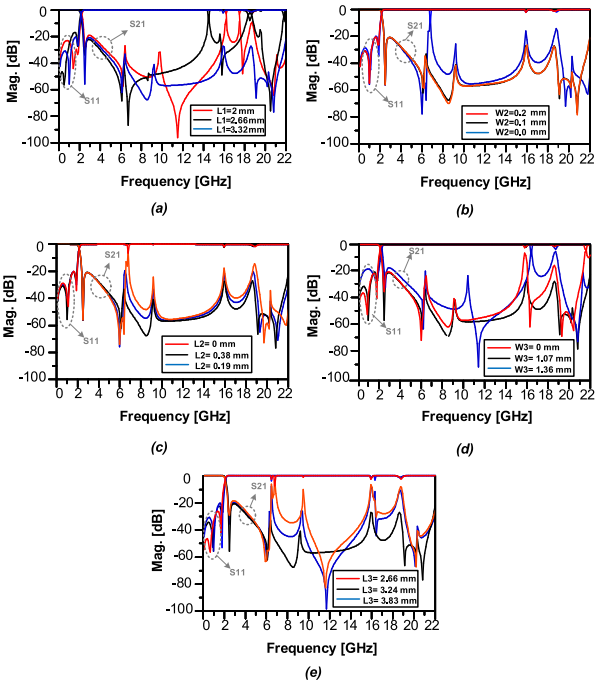

FIGURE 2. Calculated frequency response with different size of dimensions. (a) Different values of L_1 (b) Different values of W_2 (c) Different values of L_2 (d) Different values of W_3 (e) The different value of L_3.

rectangular and tapered-shaped suppressors have been implemented. Despite a high figure of merit for this filter, the return loss and consumed area require improvement. By exploiting arrow-shaped resonators and high impedance suppressing units an LPF with excellent performance is presented in [20], but this is at the expense of large size.

This paper introduces an LPF using a T-shaped resonator loaded with a stub. The proposed filter has a compact size and a simple structure. Also, a wide stopband is obtained by adding suppressing cells whilst maintaining a small size. The rest of this paper is organized as follows: Section II describes the steps of the filter design and investigates the operation of the suppressing cells. In Section III, the simulation and measurement results are presented and discussed. Finally, we conclude in Section IV.

II. RESONATOR DESIGN

A. RESONATOR ANALYSIS

Initially, a T-shaped resonator loaded with a stub is designed and optimized for a 2.15 GHz cut-off frequency. The proposed resonator and its LC equivalent circuit are exhibited in Fig. 1(a). The L_1 and C_1 values determine the cut-off frequency. The side inductors L_2 affect the suppression level. The LC values of the equivalent circuit elements can be expressed as [21] and [22]

$$L = \frac{l_L Z_L}{\upsilon_p} \tag{1}$$

$$C = \frac{\beta}{2\omega Z_C} \tanh(\beta l_C) \tag{2}$$

where, Z_L indicates the characteristic impedance of the short-line stubs and Z_C denotes the characteristic impedance of the open-circuit stubs. Here, l_L and l_C are the physical lengths. The υ_p and β signify the propagation constant and phase velocity of the transmission line, respectively. Transmission lines in microstrip circuits can have bends, gaps, impedance steps, open ends, vias, and other features in addition to being straight. These types of elements are called microstrip discontinuities. Fig. 3 displays various discontinuities of the suggested filter along with their equivalent circuits. Corners and edge-current disturbances cause shunt capacitance in bends and steps, which results in series inductances in these discontinuities. Equations (3)-(5) can be used to provide the approximate lumped values in the equivalent circuit of step discontinuities [21],

$$C_s = 0.00137h\frac{\sqrt{\varepsilon_{re1}}}{Z_{c1}}\left(1-\frac{W_2}{W_1}\right)\left(\frac{\varepsilon_{re1}+0.3}{\varepsilon_{re1}-0.258}\right) \times \left(\frac{W_1/h\ +0.264}{W_1/h\ +0.8}\right)[\text{pF}] \tag{3}$$

$$L_{s1} = \frac{L_{w1}}{L_{w1}+L_{w2}}L \tag{4}$$

$$L_{s2} = \frac{L_{w2}}{L_{w1}+L_{w2}}L. \tag{5}$$

In which ε_{re} is the effective dielectric constant of the microstrip line and h is the dielectric substrate thickness. For $i = 1, 2$

$$L_{wi} = Z_{ci}\frac{\sqrt{\varepsilon_{\text{rei}}}}{\upsilon_p} \tag{6}$$

$$L = 0.000987h\left(1-\frac{Z_{c1}}{Z_{c2}}\sqrt{\frac{\varepsilon_{re1}}{\varepsilon_{re2}}}\right)^2[\text{nH}] \tag{7}$$

$$Z_{ci} = \frac{\eta}{2\pi\sqrt{\varepsilon_{\text{rei}}}}\ln\left[\frac{F_i}{u_i}+\sqrt{1+\left(\frac{2}{u_i}\right)^2}\right] \tag{8}$$

$$\varepsilon_{\text{rei}} = \frac{\varepsilon_r+1}{2}+\frac{\varepsilon_r-1}{2}\left(1+\frac{10}{u_i}\right) \tag{9}$$

$$a_i = 1+\frac{1}{49}\ln\left(\frac{u_i^4+(u_i/52\ )^2}{u_i^4+0.432}\right) + \frac{1}{18.7}\ln\left(1+\left(\frac{u_i}{18.1}\right)^3\right) \tag{10}$$

$$b = 0.564\left(\frac{\varepsilon_r-0.9}{\varepsilon_r+3}\right)^{0.053} \tag{11}$$

$$F_i = 6+(2\pi-6)\exp\left[-\left(\frac{30.666}{u_i}\right)^{0.7528}\right] \tag{12}$$

$$u_i = \frac{W_i}{h} \tag{13}$$

where $\eta = 120\pi$ Ohms. Equations (14)-(16) are used to determine the formulas for the inductance and capacitance of bend discontinuities [21],

$$\frac{C_d}{W}[\text{pF/m}\ ] = \frac{(\varepsilon_r+12.5)\,W/h\ -(1.83\varepsilon_r-2.25)}{\sqrt{W/h}} + \frac{0.02\varepsilon_r}{W/h},\ W/h\ <1 \tag{14}$$

$$\frac{C_d}{W}[\text{pF/m}\ ] = (9.5\varepsilon_r+1.25)\,W/h + 5.2\varepsilon_r+7,\quad W/h\ >1 \tag{15}$$

$$\times\ \frac{L_d}{W}[\text{nH/m}\ ] = 100\left(4\sqrt{\frac{W}{h}}-4.21\right). \tag{16}$$

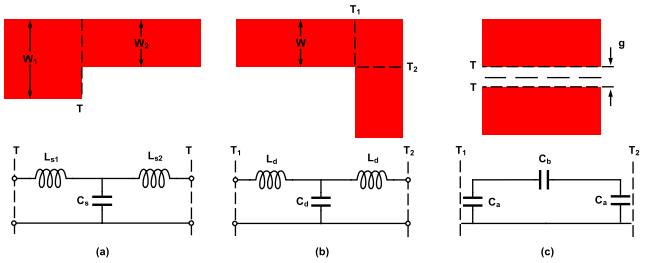

FIGURE 3. Microstrip discontinuities and their equivalent circuits; (a), step; (b), bend; and (c) gap.

There is a gap discontinuity capacitance (C_b) across to reflect the energy coupling between the open-circuit microstrip ends. Grounded capacitors (C_a) represent the fringe fields.The capacitance values in the equivalent circuit of gap discontinuities are obtained from Equations (17)-(18)

$$C_a = C_m \tag{17}$$

$$C_b = \frac{1}{2}(C_e - C_a) \tag{18}$$

where C_e and C_m stand in for electrical and magnetic walls, respectively, and represent a short and an open circuit in the equivalent circuit.

B. FILTER DESIGN

Fig. 1 shows the process of designing the filter in three steps. First, a T-shaped resonator is designed and optimized for the pre-determined frequency. As shown in Fig. 1(a), the prototype resonator has a cut-off frequency of 2.15 GHz with a suppression level of −40 dB. The cut-off frequency can be calculated as:

$$f_c = \frac{1}{2\pi\sqrt{L_1C_1}}. \tag{19}$$

Second, with the addition of open stub suppressor cell-1 as shown in Fig. 1(b), more transmission zeroes are created at low frequencies, and thereby, the stopband is improved from 2.4 GHz to 7 GHz. Finally, with the addition of another open stub suppressor cell-2 as shown in Fig. 1(c), and implementing the coupling effect between adjacent stubs, a wide stopband is achieved without increasing the size of the filter. The effect of gaps W_2 and W_3 on the stopband is shown in Fig. 2(b) and (d) respectively. As can be seen with the aid of the coupling effect as a result of these gaps more harmonics are suppressed especially at high frequencies.

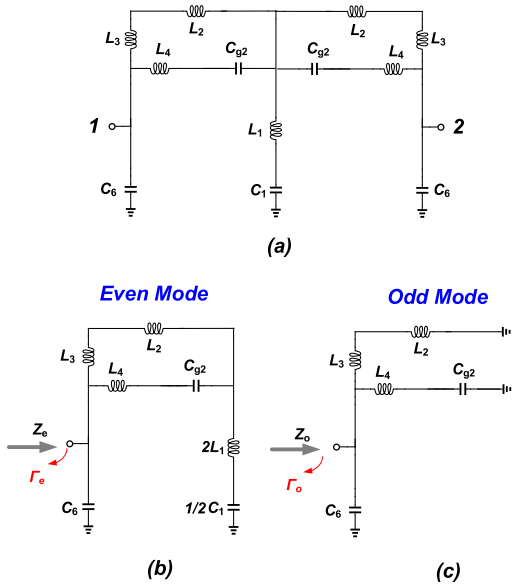

FIGURE 4. a) Simplified equivalent circuit b) Even-mode excitation c) Odd-mode excitation.

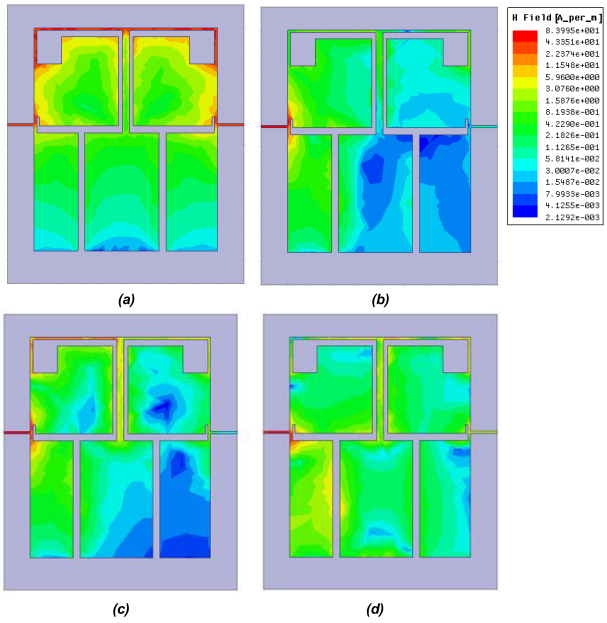

FIGURE 5. Field distribution (a) at 1 GHz (b) at 10 GHz (c) at 4 GHz (d) at 20 GHz.

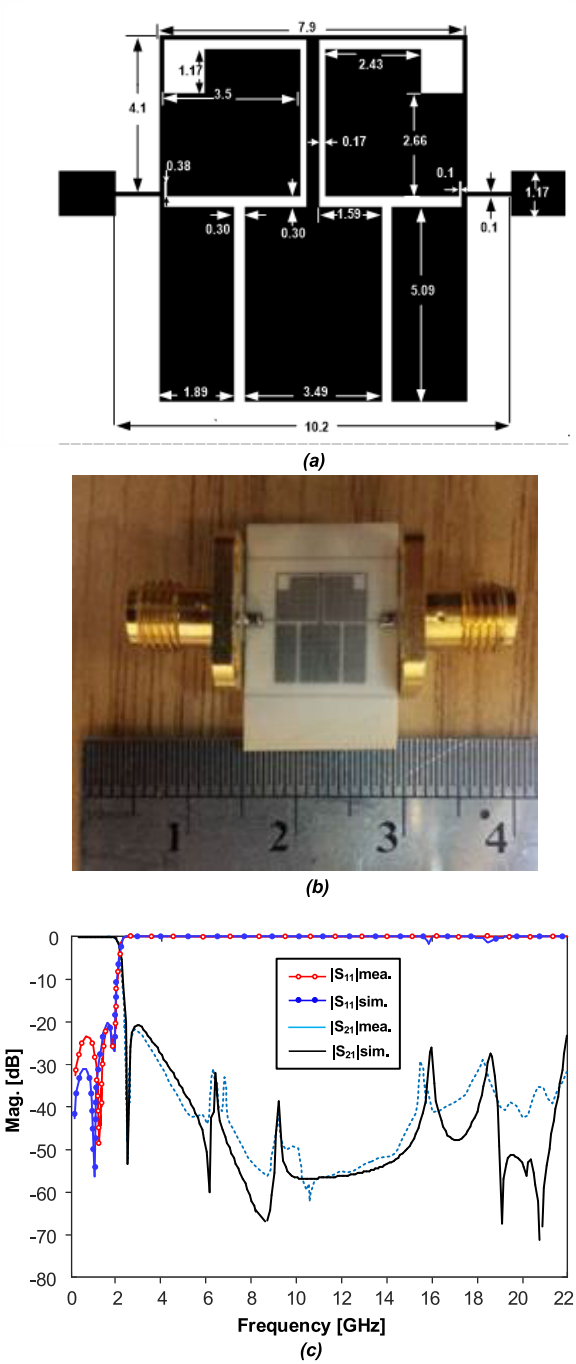

FIGURE 6. Proposed lowpass filter (a) Layout and its dimensions (unit: mm) (b) Photograph of fabricated structure (c) The simulated and measured S-parameters.

Therefore, a wide stopband is achieved without adding additional suppressing cells. The effect of other dimensions of the secondary suppressor cell, L_1, L_2, and L_3, on the final frequency response, are demonstrated in Fig. 2(a),(c) and (e), respectively. As shown in Fig. 2, the dimensions of these suppressor cells mainly affect harmonics in the stopband; therefore, the bandwidth has very little affect on S_{11} and the return loss. The desired frequency response with the sharpest roll-off and the broadest stopband is obtained using $W_1 = 1$ mm, $L_1 = 2.66$ mm, $W_2 = 0.1$ mm, $L_2 = 0.38$ mm, $W_3 = 0.071$ mm, $L_3 = 0.3$ mm. Agreement between EM-simulated and LC-equivalent results can be observed from Fig. 1(f).

Since the S_{21} expression of the designed filter is too complicated, to obtain transmission zeroes (f_{Z1} and f_{Z2}) shown in Fig. 1(e), the circuit is simplified as Fig. 4(a) in which elements with negligible effect on transmission zeroes have been eliminated. The S_{21} scattering parameter can be derived using even-odd mode analysis due to symmetry of equivalent circuit [21]. The S_{21} expression of the simplified circuit can

TABLE 1. Performance comparisons between the proposed filter and other works.

References	f_c (GHz)	ξ (dB/GHz)	NCS $(\lambda_g{}^2)$	RSB	RL	SF	AF	Size (mm^2)
[1]	1.4	68	0.0073	1.86	13	2.2	1	189.84
[2]	2.11	100	0.0320	1.59	13.5	2	1	196.85
[3]	1.65	57.8	0.0120	1.61	11	3.5	1	529.2
[4]	1.8	45.1	0.0200	1.33	20	4	1	2083.96
[5]	2.2	14.2	0.0272	1.26	NA	3	1	NA
[6]	3.11	171.5	0.1540	1.12	15	2.5	2	232.32
[7]	1.44	90.24	0.0053	1.65	14	2	1	132
[9]	3.37	188.9	0.0504	0.9	NA	2	1	79.98
[10]	1.24	336.4	0.0150	1.33	14	1.93	1	NA
[11]	2.11	340	0.0280	1.7	16	2.8	1	283.5
[12]	1.96	104	0.0229	1.8	12	2	1	213.44
[13]	5.15	47.22	0.063	1.56	10	2	1	113
[14]	3.8	25.37	0.018	1.34	14	2	1	63
[15]	2.15	123	0.0195	1.529	20	2	1	194.56
[18]	0.86	154	0.012	1.54	NA	4	1	211.12
[19]	1.83	211.1	0.013	1.65	18.1	2	1	200
This Work	**2.15**	**123**	**0.0132**	**1.6**	**20**	**2**	**1**	**96.8**

be calculated as follows:

$$S_{21} = \frac{1}{2(\Gamma_e - \Gamma_o)} = \frac{(Z_e - Z_o)Z_s}{(Z_e + Z_s)(Z_o + Z_s)} \tag{20}$$

in which Γ_e and Γ_o are even and odd-mode reflection coefficients for the even-odd mode circuits in Fig. 4. Here, Z_s, Z_e and Z_o are source impedance, even- and odd-mode input impedance, respectively. The transmission zeros of the LC equivalent circuit can be found by solving the following equations:

$$Z_e - Z_o = 0 \tag{21}$$

in which

$$Z_e = \frac{Z_x}{Z_x C_6 s + 1} \tag{22}$$

$$Z_x = \frac{2}{C_1 s} + 2L_1 s + \frac{((L_2 + L_3)s)(L_4 s + \frac{1}{C_{g2}s})}{(L_2 + L_3 + L_4)s + \frac{1}{C_{g2}s}} \tag{23}$$

$$Z_o = \frac{1}{(\frac{1}{(L_2+L_3)s} + \frac{1}{L_4 s + \frac{1}{C_{g2}s} + \frac{1}{C_6 s}})}. \tag{24}$$

With the aid of equations (20)–(24), transmission zeros are obtained.

In order to study the behavior of the filter in the passband and stopband, the electromagnetic field distribution is simulated using the High Frequency Structure Simulator (HFSS) at four frequencies. The field distribution of the filter at frequencies 1 GHz and 10 GHz is shown in Fig. 5(a) and (b) respectively, in which one of them is in the middle of the passband and the other is in the middle of the stopband. At a frequency of 1 GHz, the total RF energy is transmitted from the input port to the output port. At 10 GHz, almost all RF energy is blocked at the input; consequently, no transmission reaches the output. For further investigation, the electromagnetic field distribution of the filter at two other frequencies (4 GHz and 20 GHz) in the stopband is shown in Fig. 5(c) and (d) respectively. As obviously seen, almost the same behavior exists for all of stopband frequencies and RF energy is blocked at the input.

III. FABRICATION AND MEASURED RESULTS

The filter is implemented on RT/Duroid5880 with relative dielectric constant $\varepsilon_r = 3.38$, thickness $h = 0.508$ mm and loss tangent $= 0.0021$. The layout and photograph of the fabricated filter are shown in Fig. 6(a) and Fig. 6(b), respectively. The measurement is performed on an Agilent E8363B network analyzer. As shown in Fig. 6(c), there is conformity between simulation and measured results. The stopband is found to be from 2.4 to 22.1 GHz with a rejection level lower than −20 dB deduced by simulation. The roll-off rate from −3 dB cut-off frequency to −40 dB is 123 dB/GHz, and return loss is less than −20 dB. All of the aforementioned desired features are achieved with a compact size under 100 mm^2. A flat group delay in the passband region is important for an LPF, because group delay variations increase the phase distortion. The group delay response of the proposed filter is shown in Fig. 7. As can be seen, it has a maximum variation of less than 0.9 ns in 90% of the passband region. This low amount of variation is desired to increase the filter's immunity to phase distortion. The comparison of performance between the proposed filter with other studies is shown in Table 1, where parameters such as relative stopband (RSB), normalized circuit size (NCS), suppression factor (SF), and roll-off rate (ξ) as defined in [2] are compared. Our fabricated LPF has the smallest size compared to previous studies except [9], [14]. The importance of size of LPFs is crucial in phased array applications. In [9] the NCS is $0.0504\lambda_g{}^2$; however in our work it has improved to as little as $0.0132\lambda_g{}^2$.

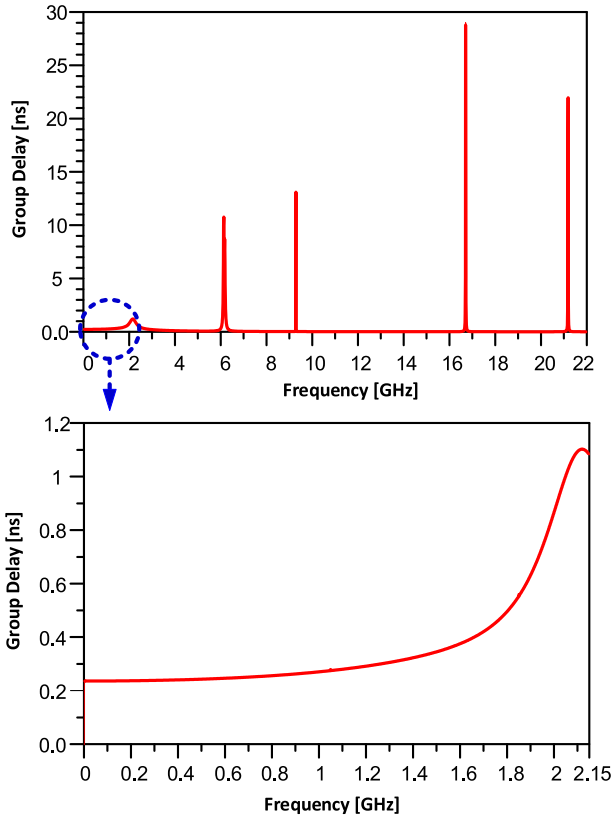

FIGURE 7. The group delay response of the proposed filter.

Moreover, the stopband in [9] is not wide enough. The RSB in [9] is 0.9 while in our work it is 1.6. In [14] both roll-off rate and RSB are not adequate. Also in [14], the roll-off rate (ξ) is 25.37 but our proposed structure has a sharp roll-off equal as high as 123 dB/GHz. Whilst maintaining a compact size, we obtain a sharp roll-off and wide stopband exploiting a T-shaped resonator and coupling effect between adjacent stubs, respectively.

IV. CONCLUSION

An LPF with a simple structure with an area smaller than 100 mm^2, return loss lower than -20 dB, wide stopband from 2.4 to 22.1 GHz, and sharp roll-off has been designed, fabricated, and measured. The validity of this filter is demonstrated via agreement between simulation, analytical, and measured results. Compared with other LPFs, our filter has a very simple structure and has potential application in microwave communication systems.

REFERENCES

[1] M. Hayati, M. Najafi, F. Shama, and S. Zarghami, "Microstrip lowpass filter with ultra-wide stopband using folded structures," *Frequenz*, vol. 73, nos. 5–6, pp. 219–226, May 2019.
[2] T. K. Rekha, P. Abdulla, P. M. Jasmine, and A. R. Anu, "Compact microstrip lowpass filter with high harmonics suppression using defected structures," *AEU-Int. J. Electron. Commun.*, vol. 115, Feb. 2020, Art. no. 153032.
[3] B. Zhang, S. Li, and J. Huang, "Compact lowpass filter with wide stopband using coupled rhombic stubs," *Electron. Lett.*, vol. 51, no. 3, pp. 264–266, 2015.
[4] V. K. Velidi and S. Sanyal, "High-rejection wide-stopband lowpass filters using signal interference technique," *Int. J. RF Microw. Comput.-Aided Eng.*, vol. 20, no. 3, pp. 253–258, May 2010.
[5] Z. Du, H. Yang, H. Zhang, and M. Zhu, "Compact lowpass filter with high suppression level and wide stopband using stepped impedance m-shape units," *Microw. Opt. Technol. Lett.*, vol. 56, no. 12, pp. 2947–2950, 2014.
[6] Q. Li, Y. Zhang, D. Li, and K. Xu, "Compact low-pass filters with deep and ultra-wide stopband using tri- and quad-mode resonators," *IET Microw., Antennas Propag.*, vol. 11, no. 5, pp. 743–748, Feb. 2017.
[7] M. Ekhteraei, M. Hayati, A. H. Kazemi, and S. Zarghami, "Design and analysis of a modified rectangular-shaped lowpass filter based on LC equivalent circuit," *AEU-Int. J. Electron. Commun.*, vol. 126, Nov. 2020, Art. no. 153290.
[8] M. Hayati, M. Akbari, and R. Salahi, "Compact microstrip lowpass filter with wide stopband and very-sharp roll-off," *Electron. Lett.*, vol. 52, no. 10, pp. 830–831, May 2016.
[9] M. Xiao, G. Sun, and X. Li, "A lowpass filter with compact size and sharp roll-off," *IEEE Microw. Wireless Compon. Lett.*, vol. 25, no. 12, pp. 790–792, Dec. 2015.
[10] K. V. Phani Kumar and S. S. Karthikeyan, "Microstrip lowpass filter with flexible roll-off rates," *AEU-Int. J. Electron. Commun.*, vol. 86, pp. 63–68, Mar. 2018.
[11] A. Vaezi and F. G. Gharakhili, "Design and fabrication of microstrip lowpass filter using asymmetric hairpin resonator," *Int. J. RF Microw. Comput.-Aided Eng.*, vol. 29, no. 7, Mar. 2019, Art. no. e21733.
[12] S. Jiang and J. Xu, "Sharp roll-off planar lowpass filter with ultra-wide stopband up to 40 GHz," *Electron. Lett.*, vol. 53, no. 11, pp. 734–735, 2017.
[13] A. Kolahi and F. Shama, "Compact microstrip low pass filter with flat group-delay using triangle-shaped resonators," *AEU-Int. J. Electron. Commun.*, vol. 83, pp. 433–438, Jan. 2018.
[14] B. Hiedari and F. Shama, "A harmonics suppressed microstrip cell for integrated applications," *AEU-Int. J. Electron. Commun.*, vol. 83, pp. 519–522, Jan. 2018.
[15] S. Liu, J. Xu, and Z. Xu, "Compact lowpass filter with wide stopband using stepped impedance hairpin units," *Electron. Lett.*, vol. 51, no. 1, pp. 67–69, 2015.
[16] L. Ge, J. P. Wang, and Y.-X. Guo, "Compact microstrip lowpass filter with ultra-wide stopband," *Electron. Lett.*, vol. 46, no. 10, pp. 689–691, May 2010.
[17] Z. Du, H. Yang, H. Zhang, and M. Zhu, "Compact LPF with sharp roll off and wide stopband using coupling stepped impedance triangular resonator," *Prog. Electromagn. Res. Lett.*, vol. 44, pp. 29–34, 2014.
[18] Q. He and C. Liu, "A novel low-pass filter with an embedded band-stop structure for improved stop-band characteristics," *IEEE Microw. Wireless Compon. Lett.*, vol. 19, no. 10, pp. 629–631, 2009.
[19] M. Hayati, S. M. Mustafa, F. Shama, and H. Abbasi, "Ultra-wide stopband lowpass filters using ring resonators," *Int. J. Microw. Wireless Technol.*, vol. 13, no. 9, pp. 880–886, Mar. 2021.
[20] S. H. Kazemi, M. Ghanbarpour, A. Zahedi, and M. Hayati, "A microstrip lowpass filter with sharp roll-off using arrow-shaped resonators and high-impedance open stubs," *AEU-Int. J. Electron. Commun.*, vol. 136, Jul. 2021, Art. no. 153775.
[21] Z. Awang, *Microwave Systems Design*. Cham, Switzerland: Springer, 2014.
[22] J. G. S. Hong and M. J. Lancaster, *Microstrip Filters for RF/Microwave Applications*. Hoboken, NJ, USA: Wiley, 2004.

MOHSEN HAYATI received the B.E. degree in electronics and communication engineering from Acharya Nagarjuna University, Andhra Pradesh, India, in 1985, and the M.E. and Ph.D. degrees in electronics engineering from Delhi University, Delhi, India, in 1987 and 1992, respectively. In 1993, he joined the Department of Electrical Engineering, Razi University, Kermanshah, Iran, as an Assistant Professor, where he is currently a Professor. He has published more than 300 papers in international and domestic journals and conferences. His current research interests include microwave and millimeter-wave devices and circuits, the application of computational intelligence, artificial neural networks, fuzzy systems, neuro-fuzzy systems, electronic circuit synthesis, and modeling and simulations.

REZVAN SALAHI was born in Kermanshah, Iran, in 1993. She received the B.Sc. and M.Sc. degrees (Hons.) in electrical engineering (electronics) from Razi University, Iran, in 2015 and 2017, respectively. She is currently pursuing the Ph.D. degree in electrical engineering with the Amirkabir University of Technology (Tehran Polytechnic), Iran. Her research interests include microstrip filters, high-frequency circuit design, wireless power transfer links, and ultrasound imaging of biomedical implants.

MARYAM AKBARI was born in Kermanshah, Iran, in 1993. She received the B.Sc. and M.Sc. degrees from Razi University, Iran, in 2015 and 2017, respectively. She is currently pursuing the Ph.D. degree with the Iran University of Science and Technology (IUST), Iran. Her research interests include microstrip filters, high-frequency circuit design, physically unclonable functions (PUFs), true random number generators, and emerging technologies.

SIAMAK ZARGARI was born in Tabriz, Iran, in 1995. He received the B.Sc. and M.Sc. degrees (Hons.) from the Amirkabir University of Technology (Tehran Polytechnic), Iran, in 2017 and 2019, respectively, where he is currently pursuing the Ph.D. degree in electrical engineering. His research interests include microstrip filters, high-frequency circuit design, medical instrumentation and circuit design for biomedical applications, high-speed, low-power, and area-efficient CMOS analog circuits, and RF building blocks.

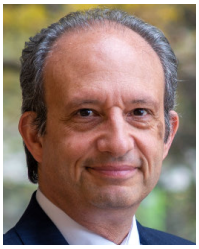

DEREK ABBOTT (Fellow, IEEE) was born in South Kensington, London, U.K. He received the B.Sc. degree (Hons.) in physics from Loughborough University, Leicestershire, U.K., in 1982, and the Ph.D. degree in electrical and electronic engineering from The University of Adelaide, Adelaide, SA, Australia, in 1997, under the supervision of Kamran Eshraghian and Bruce R. Davis. His research interests include multidisciplinary physics and electronic engineering applied to complex systems. His research programs span a number of areas of stochastic, game theory, circuits, photonics, energy policy, biomedical engineering, and computational neuroscience. He is a fellow of the Institute of Physics, U.K., and an Honorary Fellow of Engineers Australia. He was a recipient of a number of awards, including the South Australian Tall Poppy Award for Science, in 2004, the Australian Research Council Future Fellowship, in 2012, the David Dewhurst Medal, in 2015, the Barry Inglis Medal, in 2018, and the M. A. Sargent Medal for eminence in engineering, in 2019. He was an Editor and/or the Guest Editor for a number of journals, including IEEE JOURNAL OF SOLID-STATE CIRCUITS, *Journal of Optics B*, *Chaos*, *Fluctuation and Noise Letters*, PROCEEDINGS OF THE IEEE, and the IEEE PHOTONICS JOURNAL. He has served on the Board of the PROCEEDINGS OF THE IEEE. He is currently on the editorial boards of the *Scientific Reports* (Nature), *Royal Society OS*, *Frontiers in Physics PNAS Nexus*, and IEEE ACCESS. He serves on the IEEE Publication Services and Products Board (PSPB) and is the current Editor-in-Chief (EIC) for IEEE ACCESS.